JACS
JOURNAL OF THE AMERICAN CHEMICAL SOCIETY

Communication

pubs.acs.org/JACS

Charge Carrier Dynamics of Vapor-Deposited Small-Molecule/Fullerene Organic Solar Cells

Angela Y. Chang,[†] Yi-Hong Chen,[‡] Hao-Wu Lin,[‡] Li-Yen Lin,[§] Ken-Tsung Wong,[§] and Richard D. Schaller*[,†,⊥]

[†]Department of Chemistry, Northwestern University, Evanston Illinois 60208, United States

[‡]Department of Materials Science and Engineering, National Tsing-Hua University, Hsin Chu 30013, Taiwan

[§]Department of Chemistry, National Taiwan University, Taipei 10617, Taiwan

[⊥]Center for Nanoscale Materials, Argonne National Laboratory, Argonne, Illinois 60439, United States

Supporting Information

ABSTRACT: Although small-molecule organic solar cells (SMOSCs) have shown increasingly promising prospects as a source of solar power, there have been few studies concerning the photophysics of these systems. Here, we report the time scale and efficiency of charge separation and recombination in a vapor-deposited SMOSC material that produces 5.81% power conversion efficiency. Transient absorption and time-resolved photoluminescence (trPL) studies of thin film blends comprising DTDCTB, a narrow-band gap electron donor, and either C_{60} or C_{70} as an electron acceptor show that charge separation occurs in ∼100 fs, while charge recombination takes place over sub-ns and ns time scales. trPL indicates a donor electron−hole pair lifetime of ∼33 ps in the neat film and reveals that ∼20% of donors fail to charge separate in donor−acceptor mixed films, likely owing to some spatially extended donor-rich regions that interact poorly with acceptors. Our results suggest that morphological manipulations of this material could further improve device efficiency.

Organic solar cells (OSCs) have emerged as a promising alternative to crystalline inorganic photovoltaics due to their low cost, light weight, mechanical flexibility, and scalability.[1] Much effort has focused on devices that utilize semiconducting polymers as electron donors and fullerenes or fullerene derivatives as electron acceptors. Such polymer-based devices have achieved power conversion efficiencies (PCEs) of 9−10.6%.[2,3] More recently, small-molecule OSCs (SMOSCs) have gained attention due to their well-defined molecular structures, easier purification, and better batch-to-batch reproducibility as compared to polymeric materials.[4,5] To date, single-junction SMOSCs have achieved PCEs of 6.8−8%,[6−8] and with their rapid pace of improvement they may soon eclipse the performance of polymer-based devices.

Concomitant with improvements in OSC design and fabrication have been many studies examining the photophysics of the active layer to better understand how molecular structure influences device efficiency. Numerous differences exist between polymer and small molecule-based OSCs that can affect charge movement. For instance, polymeric donors offer spatially extended intrachain electronic orbitals that impact rates and efficiency of charge separation and recombination, whereas small molecules lack this feature.[9] Additionally, in polymer-based devices, the bulk heterojunction (BHJ), a bicontinuous interpenetrating network of relatively pure donor and acceptor domains, constitutes the active layer. However, in small molecule-based devices the BHJ is replaced with the mixed heterojunction (MHJ) or molecular BHJ, which may not contain truly bicontinuous or interpenetrating donor and acceptor domains.[4,10] Such morphology differences might yield largely disparate charge-transfer time scales for these two classes of photovoltaic materials. Using techniques such as transient absorption (TA) and time-resolved photoluminescence (trPL), researchers have observed ultrafast charge separation and recombination in polymeric systems[11−17] and considered the effect of nanoscale morphology on charge transport.[18−22] In comparison, few investigations into the photophysics of SMOSCs exist,[23−25] resulting in a less complete understanding as to how SMOSC devices produce high PCEs.

Recently, Lin and co-workers et al. demonstrated high PCE (5.81%) in a SMOSC using the donor−acceptor−acceptor molecule 2-{[7-(5-*N*,*N*-ditolylaminothiophen-2-yl)-2,1,3- benzothiadiazol-4-yl]methylene}malononitrile (DTDCTB) in conjunction with C_{60} or C_{70}.[26] Despite the achievement of efficient devices using this donor moelcule,[27,28] to date there has been little investigation of the underlying photophysics of this system and thus limited understanding as to charge separation and recombination timescales. Here, we report TA and trPL studies that establish carrier dynamics in thin films of DTDCTB:C_{60} and DTDCTB:C_{70} that yield high PCE.[26] Using spectrally resolved TA from the visible through the NIR, we observe correlated, sub-ps charge separation times and multiple timescales of charge recombination. Consistent with our reported ultrafast charge separation times, trPL shows that the donor excited state is short-lived (∼33 ps), indicating that fast charge separation is important for efficient device performance. trPL also reveals that ∼20% of donor molecules fail to charge separate, likely due to the morphology of the

Received: March 27, 2013
Published: May 29, 2013

   dx.doi.org/10.1021/ja403056y | *J. Am. Chem. Soc.* 2013, 135, 8790−8793

active layer, which suggests material manipulations may improve PCEs.

Thin films of DTDCTB, C_{60}, C_{70}, DTDCTB:C_{60}, and DTDCTB:C_{70} were prepared using previously reported techniques.[26] Sample specifications and experimental details on UV–vis, TA, and trPL measurements may be found in the Supporting Information (SI). UV–vis absorption spectra of thin film samples of DTDCTB, C_{60}, C_{70}, 1:1 DTDCTB:C_{60}, and 1:1.6 DTDCTB:C_{70} are shown in Figure 1. Spectra were

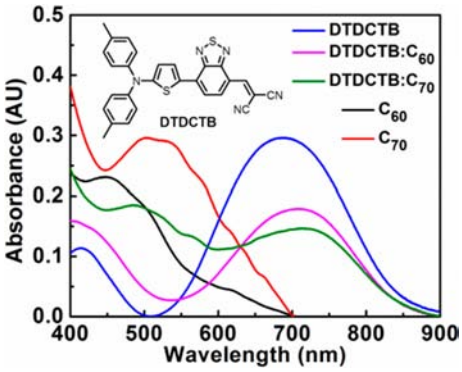

Figure 1. Absorption spectra of C_{60}, C_{70}, DTDCTB (structure inset), DTDCTB:C_{60}, and DTDCTB:C_{70}.

corrected for reflection loss of the glass substrate. DTDCTB exhibits a broad absorption feature with a peak at 688 nm and FWHM of 188 nm. The measured absorption spectra of DTDCTB:C_{60} and DTDCTB:C_{70} could not be exactly replicated via superposition of the spectra of the separate components in their given ratios (Figure S1). Based on the absorption spectra we chose 750 to 800 nm as the pump wavelengths with which to investigate these materials. In particular, the donor exhibits absorbance in this range while the acceptor molecules do not, such that we can selectively excite the donor to simplify data interpretation. All presented TA studies were performed under N_2.

The fsTA spectra of (a) DTDCTB, (b) DTDCTB:C_{60}, and (c) DTDCTB:C_{70} are presented in Figure 2 for indicated time delays and are truncated from 775 to 825 nm due to overlap with the laser fundamental (800 nm pump at 62 μJ/cm^2). Films of C_{60} or C_{70} did not produce discernible TA signals (not shown), which confirmed selective excitation of the donor. Neat DTDCTB films (Figure 2a) exhibit a photoinduced absorption (PIA) at 535 nm, a broad bleach between 585 and 775 nm, and a weak, featureless PIA in the NIR region. We note that the bleach feature arises from state filling (electron populating the LUMO) rather than stimulated emission, as it occurs at higher energy than the excitation. The largest amplitude changes in the spectra occur by 1 ps delay time; further increases in the delay yield decreasing signal strength for both the 535 nm PIA (likely associated with a DTDCTB radical cation signal contribution, as this feature does not become weaker upon electron transfer to fullerenes) and the bleach feature.

The introduction of C_{60} or C_{70} results in several significant changes in the fsTA spectra. For both DTDCTB:C_{60} and DTDCTB:C_{70} films, the signal at 651 nm decreases substantially in comparison to the neat DTDCTB film (Figure 2a,b, left box). Additionally, the broad PIA in the NIR range exhibits a greater intensity, and a strong bleach remains between 685 and 775 nm. For DTDCTB:C_{60} (Figure 2b), two distinct PIAs occur at 553 and 1064 nm, and the latter is absent for neat DTDCTB films (Figure 2a,b, right box). TA spectra of DTDCTB:C_{70} (Figure 2c) show a PIA at 553 nm with a shoulder at 585 nm and a PIA at 898 nm (Figure 2c, right box). PIA at 898 nm occurs in neat DTDCTB but with less intensity (Figure 2a, center box).

Based on our observations of the fsTA spectra, we further investigated the dynamics at 651, 898, and 1064 nm in Figure 3. Figure 3a shows the time traces for each of the three films at 651 nm through 2 ps. We see that the bleach in the neat DTDCTB film rises within 500 fs, and by fitting a single exponential we obtained a rise time constant of 98 ± 6 fs for DTDCTB. For DTDCTB:C_{60}, the bleach amplitude is significantly reduced relative to the neat donor, and for DTDCTB:C_{70}, the initial bleach instead appears as a PIA. These changes in the donor–acceptor mixtures occurred on a timescale that could not be distinguished from our instrument response function (~100 fs). The presence of C_{60} or C_{70} acceptor molecules caused a faster decay in the donor bleach signal compared to the neat donor film, and as a result we attribute loss of the bleach feature at 651 nm to the electron leaving the donor. We identified correlated dynamics of the electron appearing on the acceptor at 1064 nm for DTDCTB:C_{60} and at 898 nm for DTDCTB:C_{70}, which further supports ultrafast (<100 fs) charge separation time scales for both systems. Literature spectroelectrochemistry reports indicate that solvated C_{60}^- exhibits a narrow spectral feature peaked at 1076 nm,[29] close to the observed PIA feature at 1064 nm in the DTDCTB:C_{60} film, and thus we attribute the instrument-limited formation of the PIA feature to the formation of C_{60}^- (Figure 3b). Literature also indicates that

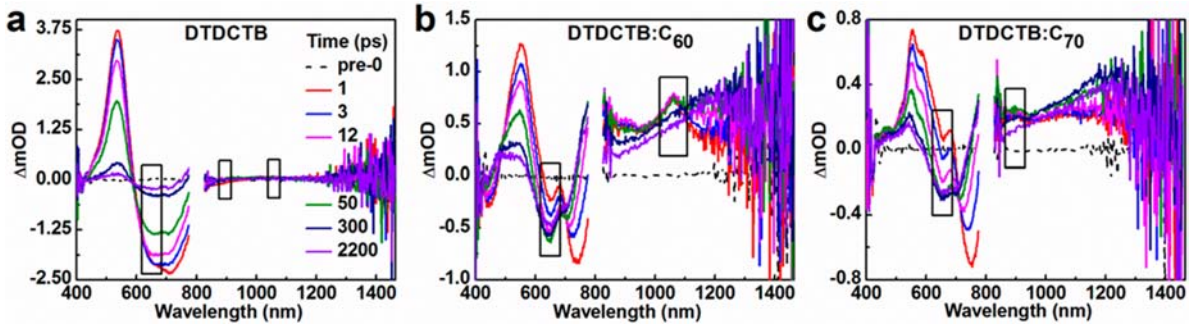

Figure 2. fsTA spectra at indicated time delays for (a) DTDCTB, (b) DTDCTB:C_{60}, and (c) DTDCTB:C_{70}. Boxed regions indicate key spectra features at 651, 898, and 1064 nm that correspond to charge separation dynamics.

dx.doi.org/10.1021/ja403056y | J. Am. Chem. Soc. 2013, 135, 8790–8793

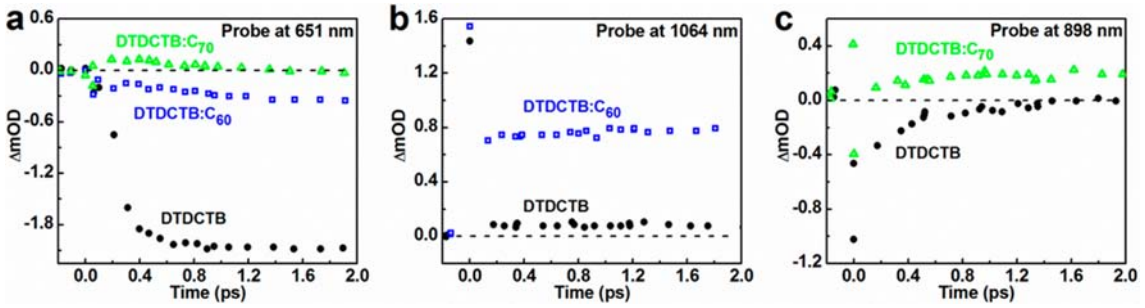

Figure 3. fsTA dynamics of DTDCTB, DTDCTB:C_{60}, and DTDCTB:C_{70} through 2 ps. (a) Dynamics at 651 nm correspond to the electron leaving the donor. (b) Dynamics at 1064 nm convey C_{60}^- formation. (c) Dynamics at 898 nm signify C_{70}^- formation.

solvated C_{70}^- produces a broad absorption feature ranging from ~1250 to 1450 nm, but otherwise exhibits moderate and featureless absorption in the NIR.[30] We attempted to investigate the dynamics at 1300 nm, however our measurements of these films yielded low signal-to-noise in this wavelength range. We found that the dynamics at 898 nm displayed sufficiently different behavior between DTDTCB:C_{70} and the donor-only film to suggest C_{70}^- formation; Figure 3c shows that while neat DTDCTB exhibits a short-lived bleach, the signal from DTDCTB:C_{70} rapidly evolves from a bleach into a PIA feature at this wavelength.

From a device perspective, it is valuable to understand the time scale of charge recombination. From fsTA measurements, we fit through 7 ns and obtained decay constants of 335 ± 92 ps for DTDCTB:C_{60} (at 1064 nm) and 336 ± 150 ps for DTDCTB:C_{70} (at 898 nm). The fluence independence of this decay constant (see Figure S2) suggests geminate recombination of charge carriers on this time scale. Longer-lived signals were measured with μsTA (using 750 nm pump at 90 μJ/cm^2). Because the largest signal-to-noise for all three samples was between 900 and 1000 nm with very little signal beyond 1300 nm, we chose 948 nm as the wavelength at which to analyze long time dynamics (Figure 4). We justify this choice of probe

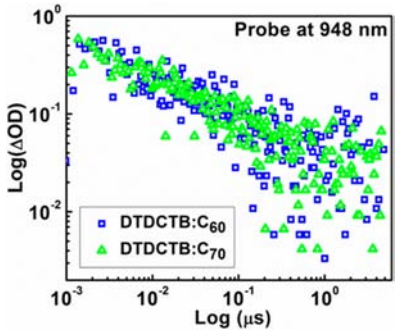

Figure 4. μsTA dynamics of DTDCTB:C_{60} and DTDCTB:C_{70} at 948 nm reveal nongeminate recombination dynamics.

wavelength with the following reasons: (1) We observe in Figure 2 that at 948 nm the donor–acceptor mixtures show much larger signals than the neat donor; and (2) an analysis of μsTA dynamics at 1209 nm showed similar results (Figure S3), indicating that the observed dynamics were not particular to this one wavelength. We fit the time traces using a biexponential decay and obtained time constants of 85.6 ± 19.2 and 496 ± 131 ns for DTDCTB:C_{60} and 59.2 ± 10.2 and 647 ± 119 ns for DTDCTB:C_{70}. The timescales of charge recombination in these two systems are comparable, likely due to the similarity of the HOMO and LUMO levels in solid-C_{60} and solid-C_{70}[31,32] as well as the comparable film morphology.[26] Furthermore, in this temporal and spectral range we clearly observe fluence-dependent dynamics and thus assign these time constants to nongeminate recombination (see Figure S2b).

To further probe the dynamics of this donor–acceptor system, we performed trPL measurements using a streak camera (excitation at 690 nm, monitored sample emission centered ~835 nm). The spectrally integrated decay dynamics shown in Figure 5a were corrected for small differences in

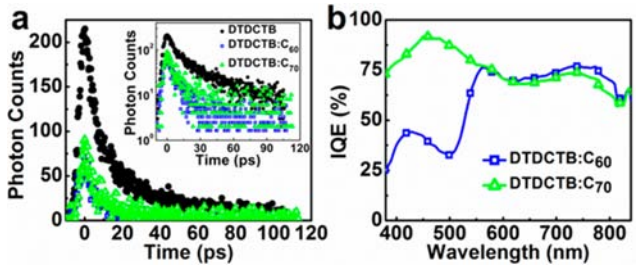

Figure 5. (a) trPL of DTDCTB emission shows weaker absolute PL intensity from mixed films compared to neat donor (semilog plot is inset). Integration indicates that ~20% of donors do not charge separate. (b) IQE of DTDCTB:C_{60} and DTDCTB:C_{70} devices (see also Figures S4–S6).

measured sample absorbance. Neat DTDCTB (solid circles) showed larger absolute intensity of the PL signal compared to the donor–acceptor mixtures (open squares and triangles). The neat donor film was found to decay with a biexponential profile that could be fitted with time constants of 7.5 ± 0.3 ps (influenced by instrument response) and 33.4 ± 5.7 ps. We note that such rapid PL decay suggests that the fast observed rates of charge separation are, in fact, requisite for efficient device performance in this instance. For DTDCTB:C_{60} and DTDCTB:C_{70} we obtained similar decay profiles as the neat donor films, which suggests that iso-energetic emission arises from DTDCTB molecules that fail to charge separate to the acceptor. Given the instrument response function of the streak camera, the loss in absolute PL intensity at early time is consistent with the sub-ps charge separation rates we observed in fsTA data. By time integrating the trPL traces, we found that the donor–acceptor mixtures emit ~20% of the photons produced by the neat DTDCTB film, which indicates that this same percentage of donors did not charge separate upon excitation. Comparing this value with the measured internal quantum efficiency (IQE) of DTDCTB-based devices, which is ~75% at 690 nm (Figure 5b), it appears that failure to charge

dx.doi.org/10.1021/ja403056y | J. Am. Chem. Soc. 2013, 135, 8790–8793

separate represents a significant percentage of the deviation of IQE from unity. The inability of some DTDCTB electron–hole pairs to charge separate likely relates to details of the mixed heterojunction (MHJ) and film microstructure, similar to variations in performance found in polymer-based devices.[18−22] In particular, if some domains of phase-separated donor molecules exceed ∼12 nm, twice the theoretical exciton diffusion length of DTDCTB, such electron–hole pairs will fail to efficiently transfer electrons to acceptor molecules.[26] This observation suggests that improvements to the morphology of the MHJ may further increase PCE in this class of device.

In conclusion, we spectroscopically characterized the time-scales of charge separation and recombination in thin films of DTDCTB, DTDCTB:C_{60}, and DTDCTB:C_{70}. We found that charge separation occurs on a 100 fs time scale, while charge recombination takes place on sub-ns and ns time scales. Streak camera measurements showed that the donor electron–hole pair state has a lifetime of only ∼33 ps, which indicates that ultrafast charge separation is indeed necessary for efficient device performance. In comparison, P3HT, a common polymeric electron donor, offers a 600 ps excited-state lifetime[33] in addition to both a slow (∼10 ps) and fast (100 fs) charge separation component, where the slower charge separation process arises from exciton migration to the donor–acceptor interface.[34] Additionally, we showed that ∼20% of donors do not charge separate after excitation, which suggests that morphological manipulations of the MHJ should help to improve device performance.

■ ASSOCIATED CONTENT

Supporting Information

Additional experimental details and figures. This material is available free of charge via the Internet at http://pubs.acs.org.

■ AUTHOR INFORMATION

Corresponding Author

schaller@anl.gov; schaller@northwestern.edu

Notes

The authors declare no competing financial interest.

■ ACKNOWLEDGMENTS

Use of the Center for Nanoscale Materials was supported by the U.S. Department of Energy, Office of Science, Office of Basic Energy Sciences, under Contract No. DE-AC02-06CH11357. We also acknowledge financial support from National Science Council of Taiwan (NSC 101-2112-M-007-017-MY3, NSC-101-2113-M-002-009-MY3) and the Low Carbon Energy Research Center, National Tsing-Hua University.

■ REFERENCES

(1) Günes, S.; Neugebauer, H.; Sariciftci, N. S. *Chem. Rev.* **2007**, *107*, 1324.

(2) He, Z.; Zhong, C.; Su, S.; Xu, M.; Wu, H.; Cao, Y. *Nat. Photonics* **2012**, *6*, 593.

(3) You, J.; Dou, L.; Yoshimura, K.; Kato, T.; Ohya, K.; Moriarty, T.; Emery, K.; Chen, C.-C.; Gao, J.; Li, G.; Yang, Y. *Nat. Commun.* **2013**, *4*, 1446.

(4) Lloyd, M. T.; Anthony, J. E.; Malliaras, G. G. *Mater. Today* **2007**, *10*, 34.

(5) Roncali, J. *Acc. Chem. Res.* **2009**, *42*, 1719.

(6) Chen, Y.-H.; Lin, L.-Y.; Lu, C.-W.; Lin, F.; Huang, Z.-Y.; Lin, H.-W.; Wang, P.-H.; Liu, Y.-H.; Wong, K.-T.; Wen, J.; Miller, D. J.; Darling, S. B. *J. Am. Chem. Soc.* **2012**, *134*, 13616.

(7) Fitzner, R.; Mena-Osteritz, E.; Mishra, A.; Schulz, G.; Reinold, E.; Weil, M.; Körner, C.; Ziehlke, H.; Elschner, C.; Leo, K.; Riede, M.; Pfeiffer, M.; Uhrich, C.; Bäuerle, P. *J. Am. Chem. Soc.* **2012**, *134*, 11064.

(8) Kyaw, A. K. K.; Wang, D. H.; Gupta, V.; Leong, W. L.; Ke, L.; Bazan, G. C.; Heeger, A. J. *ACS Nano* **2013**, *7*, 4569.

(9) Bakulin, A. A.; Rao, A.; Pavelyev, V. G.; Van Loosdrecht, P. H. M.; Pshenichnikov, M. S.; Niedzialek, D.; Cornil, J.; Beljonne, D.; Friend, R. H. *Science* **2012**, *335*, 1340.

(10) Walker, B.; Kim, C.; Nguyen, T.-Q. *Chem. Mater.* **2011**, *23*, 470.

(11) Clarke, T. M.; Durrant, J. R. *Chem. Rev.* **2010**, *110*, 6736.

(12) Tong, M.; Coates, N. E.; Moses, D.; Heeger, A. J. *Phys. Rev. B* **2010**, *81*, 125210.

(13) Banerji, N.; Cowan, S.; Leclerc, M.; Vauthey, E.; Heeger, A. J. *J. Am. Chem. Soc.* **2010**, *132*, 17459.

(14) Etzold, F.; Howard, I. A.; Mauer, R.; Meister, M.; Kim, T.-D.; Lee, K.-S.; Baek, N. S.; Laquai, F. *J. Am. Chem. Soc.* **2011**, *133*, 9469.

(15) Massip, S.; Oberhumer, P. M.; Tu, G.; Albert-Seifried, S.; Huck, W. T. S.; Friend, R. H.; Greenham, N. C. *J. Phys. Chem. C* **2011**, *115*, 25046.

(16) Piliego, C.; Loi, M. A. *J. Mater. Chem.* **2012**, *22*, 4141.

(17) Hwang, I.; Beaupré, S.; Leclerc, M.; Scholes, G. D. *Chem. Sci.* **2012**, *3*, 2270.

(18) Thompson, B. C.; Fréchet, J. M. J. *Angew. Chem., Int. Ed.* **2008**, *47*, 58.

(19) Howard, I. A.; Mauer, R.; Meister, M.; Laquai, F. *J. Am. Chem. Soc.* **2010**, *132*, 14866.

(20) Chen, W.; Xu, T.; He, F.; Wang, W.; Wang, C.; Strzalka, J.; Liu, Y.; Wen, J.; Miller, D. J.; Chen, J.; Hong, K.; Yu, L.; Darling, S. B.; Hong, O. K.; Yu, O. L. *Nano Lett.* **2011**, *11*, 3707.

(21) Botiz, I.; Schaller, R. D.; Verduzco, R.; Darling, S. B. *J. Phys. Chem. C* **2011**, *115*, 9260.

(22) Groves, C.; Reid, O. G.; Ginger, D. S. *Acc. Chem. Res.* **2010**, *43*, 612.

(23) Wilson, M. W. B.; Rao, A.; Clark, J.; Kumar, R. S. S.; Brida, D.; Cerullo, G.; Friend, R. H. *J. Am. Chem. Soc.* **2011**, *133*, 11830.

(24) Credgington, D.; Kim, Y.; Labram, J.; Anthopoulos, T. D.; Durrant, J. R. *J. Phys. Chem. Lett.* **2011**, *2*, 2759.

(25) Credgington, D.; Jamieson, F. C.; Walker, B.; Nguyen, T.-Q.; Durrant, J. R. *Adv. Mater.* **2012**, *24*, 2135.

(26) Lin, L.-Y.; Chen, Y.-H.; Huang, Z.-Y.; Lin, H.-W.; Chou, S.-H.; Lin, F.; Chen, C.-W.; Liu, Y.-H.; Wong, K.-T. *J. Am. Chem. Soc.* **2011**, *133*, 15822.

(27) Lin, H.-W.; Kang, H.-W.; Huang, Z.-Y.; Chen, C.-W.; Chen, Y.-H.; Lin, L.-Y.; Lin, F.; Wong, K.-T. *Org. Electron.* **2012**, *13*, 1925.

(28) Lin, H.-W.; Chen, Y.-H.; Huang, Z.-Y.; Chen, C.-W.; Lin, L.-Y.; Lin, F.; Wong, K.-T. *Org. Electron.* **2012**, *13*, 1722.

(29) Lawson, D. R.; Feldheim, D. L.; Foss, C. A.; Dorhout, P. K.; Elliott, M.; Martin, C. R.; Parkinson, B. *J. Electrochem. Soc.* **1992**, *139*, L68.

(30) Lawson, D. R.; Feldhiem, D. L.; Foss, C. A.; Dorhout, P. K.; Elliott, C. M.; Martin, C. R.; Parkinson, B.; Feldheim, D. L.; Michael, C. E. *J. Phys. Chem.* **1992**, *96*, 7175.

(31) Weaver, J. H. *J. Phys. Chem. Solids* **1992**, *53*, 1433.

(32) Han, B.; Yu, L.; Hevesi, K.; Gensterblum, G.; Rudolf, P.; Pireaux, J.; Thiry, P. A.; Caudano, R.; Lambin, P.; Lucas, A. A. *Phys. Rev. B* **1995**, *51*, 7179.

(33) Cook, S.; Furube, A.; Katoh, R. *Energy Environ. Sci.* **2008**, *1*, 294.

(34) Guo, J. M.; Ohkita, H.; Benten, H.; Ito, S. *J. Am. Chem. Soc.* **2010**, *132*, 6154.